catalysts

MDPI

Article

Enhanced Electrocatalytic Activity of Stainless Steel Substrate by Nickel Sulfides for Efficient Hydrogen Evolution

Jong-Sang Youn [1], Sangmin Jeong [2], Inhwan Oh [2], Sunyoung Park [2], Hien Duy Mai [2] and Ki-Joon Jeon [2,*]

[1] Department of Environmental Engineering, The Catholic University of Korea, Bucheon 14662, Korea; jsyoun@catholic.ac.kr

[2] Department of Environmental Engineering, Inha University, Incheon 22212, Korea; smjeong3268@gmail.com (S.J.); oh910611@naver.com (I.O.); 12171148@inha.edu (S.P.); hien.fasdas@gmail.com (H.D.M.)

* Correspondence: kjjeon@inha.ac.kr; Tel.: +82-32-860-7509

Received: 15 October 2020; Accepted: 2 November 2020; Published: 3 November 2020

Abstract: Water splitting is one of the efficient ways to produce hydrogen with zero carbon dioxide emission. Thus far, Pt has been regarded as a highly reactive catalyst for the hydrogen evolution reaction (HER); however, the high cost and rarity of Pt significantly hinder its commercial use. Herein, we successfully developed an HER catalyst composed of NiS_x (x = 1 or 2) on stainless steel (NiS_x/SUS) using electrodeposition and sulfurization techniques. Notably, the electrochemical active surface area(ECSA) of NiS_x/SUS was improved more than two orders of magnitude, resulting in a considerable improvement in the electrochemical charge transfer and HER activity in comparison with stainless steel (SUS). The long-term HER examination by linear scan voltammetry (LSV) confirmed that NiS_x/SUS was stable up to 2000 cycles.

Keywords: sulfurization; NiS-NiS_2; stainless steel 304; hydrogen evolution

1. Introduction

Hydrogen production via electrochemical water splitting is regarded as an ideal energy source that can potentially substitute conventional fossil fuel because of its large energy density and zero carbon dioxide emission [1–3]. Developing efficient and durable electrocatalysts with cost- effectiveness is highly desirable for the practical usage of water splitting devices. Pt-based catalysts are highly reactive toward the hydrogen evolution reaction (HER) due to the optimal binding energy with adsorbed hydrogen species formed during the HER process [4]; however, the high cost and rarity of Pt significantly hinder its commercial use. Therefore, tremendous effort has been devoted to develop earth-abundant materials that can substitute Pt in HER [5,6]. Among those, TMS (transition metal sulfides), such as nickel sulfides, appear to be a promising class of HER electrocatalysts owing to their earth abundance, remarkable HER performance, and long-term operational stability in both acidic and alkaline solutions [7–12]. For example, T. F. Hung et al. reported that the nickel sulfide nanostructure showed high electrochemical performance in HER and supercapacitors [13,14]. Nanostructured nickel sulfide was also superior to the bulk counterpart as reported by P. Liu et al. [14]. Although a number of synthetic methods for nickel sulfide (e.g., solvothermal and hydrothermal [7,9], and electrospinning [13] have been reported, it is still very important to establish an effective and simple approach to fabricate the nickel sulfide-based electrodes for HER application.

Electrode substrates are equally important in terms of HER efficiency as for the catalytically active phase deposited on the electrode surface since the electrochemical performance and operational

stability of HER electrodes can be substantially affected by the substrates used [15,16]. In this regard, stainless steel (SUS) has potential for efficient hydrogen evolution as a substrate because of its mechanical strength, corrosion resistance, cost-effectiveness, and good electrical conductivity compared to other substrates [17,18]. However, growing electrochemically active materials on the surface of SUS remains a challenging task. This is mainly because SUS is composed of many kinds of metals such as iron, nickel, molybdenum, chromium, and magnesium, and these metals can inevitably diffuse to the surface at high pressure and temperature [19]. This prevents researchers from controlling the material composition and in understanding the composition-HER performance correlation. Further, the slippery surface of SUS and the generation of hydrogen bubbles during HER result in the undesired detachment of catalysts from the SUS and the electrode eventually to lose its reactivity [20].

Herein, we directly fabricated nickel sulfide (NiS_x) nanostructures on SUS (NiS_x/SUS) with a facile method to enhance the stability of electrocatalysts on SUS and improve the electrocatalytic activity. Nickel electrodeposition was carried out to introduce a nickel overlay on the surface of SUS. The following sulfurization at relatively low temperature, while preventing the metal diffusion from SUS to the surface catalytic phase, was sufficient for the direct growth of NiS_x on the SUS. The reported synthetic approach is important to prevent the undesired detachment of NiS_x from the SUS surface during the HER process. The crystallinity, chemical composition and oxidation state, and morphologies of NiS_x/SUS were fully characterized by XRD (X-ray diffraction), XPS (X-ray photoelectron spectroscopy), and SEM (scanning electron microscopy). HER examination shows that the NiS_x/SUS led to a substantial improvement in the electrochemical activity and long-term stability in comparison with SUS.

2. Results

2.1. Characteristics of the NiS_x/SUS Electrode

Figure 1 depicts a schematic illustration of the electrode preparation via two steps. The first step, the nickel electrodeposition of SUS, was optimized at −5 mA cm^{-2} for 30 min in 1 M nickel sulfate solution for a uniform covering of nickel on SUS. The sulfurization (step 2) involved the chemical reaction between vaporized sulfur and nickel on SUS to generate NiS_x/SUS. The sulfurization temperature was set at 300 °C because lower or higher temperatures only resulted in inefficient sulfurization or electrode damage, respectively. This synthetic approach is very facile and can be easily scaled up. For comparison, SUS was also sulfurized under the same condition (see more details in the experimental section). After the sulfurization, the colors of the electrodes changed to black (NiS_x/SUS) and grey (S-SUS).

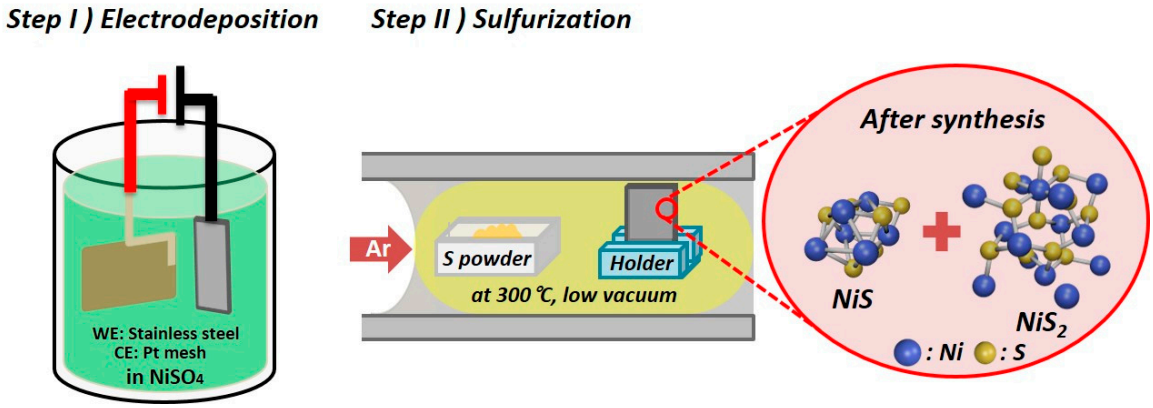

Figure 1. Schematic illustration of two-step sample preparation. Step (1) nickel electrodeposition in 1 M nickel sulfate solution and step (2) sulfurization for NiS_x/SUS at 300 °C for 30 min.

The morphological properties of the prepared samples are revealed in Figure 2. The morphology of S-SUS sparsely shows nanorod shapes lying horizontally on the SUS (Figure 2a,c). On the other hand, NiS_x/SUS was densely covered by the NiS_x nanoparticles with mean size of approx. 100 nm and thickness of approx. 24 μm. There are many more exposed active sites than for that of S-SUS (Figure 2b,d, Figure S1). These morphologies from sulfurization are consistent with previous studies [21].

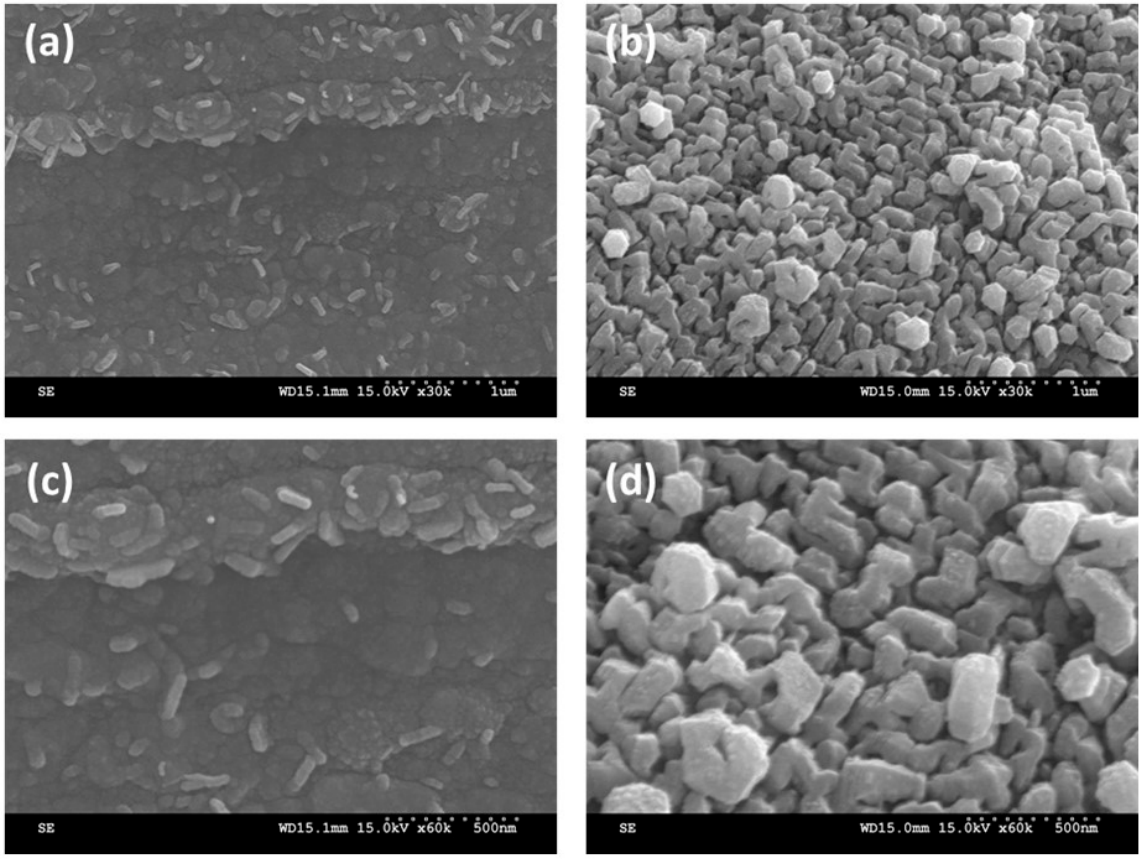

Figure 2. Typical SEM images of S-SUS (**a**,**c**) and NiS_x/SUS (**b**,**d**) at scale of 1 μm and 500 nm, respectively.

The crystallinity of the prepared electrodes was investigated using X-ray diffraction (XRD) analysis performed in the 2θ range from 20 to 90°. Figure 3 shows the XRD results of SUS, S-SUS, and NiS_x/SUS. SUS shows normal FCC (face centered cubic) crystal structure of (111), (200), and (220) at 43.5, 50.7, and 74.5° respectively, indicating consistency with previous studies [22], and there is no significant difference from XRD results between SUS and S-SUS, suggesting that SUS is relatively passive toward sulfur vapor at low temperatures. After the sulfurization of nickel on SUS, the evolution of a new set of diffraction peaks can be assigned to NiS ((100), (101), (102), and (110) at 30.1, 34.6, 45.7, and 53.5°, respectively) [7] and NiS_2 ((200), (210), (211), (220), and (311) at 31.4, 35.3, 38.8, 45, and 53.4°, respectively) [14]. The peak intensity corresponding to those characteristic of SUS is seen to lessen to some extent, implying that the surface of SUS is covered with a thick layer of NiS_x.

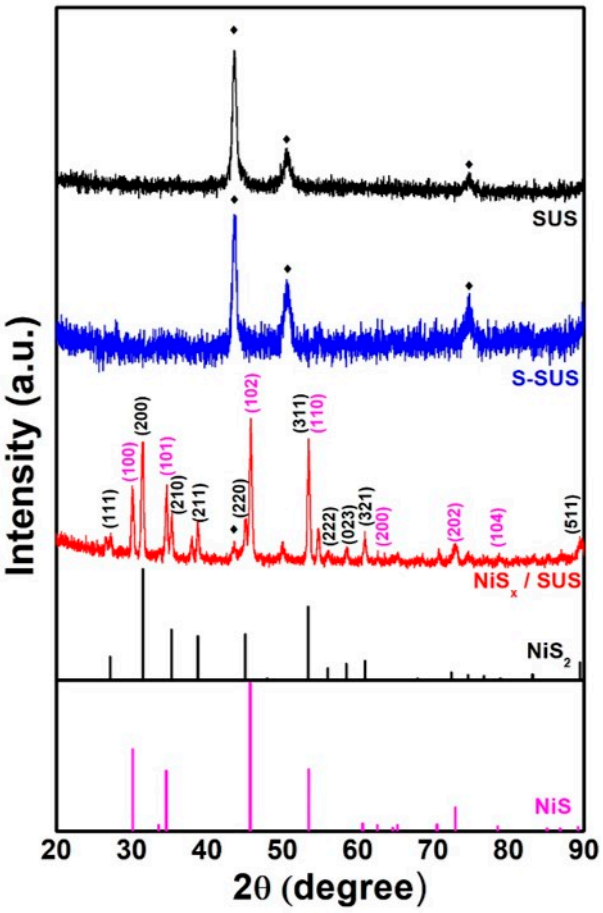

Figure 3. X-ray diffraction analysis of SUS (black), S-SUS (blue), and NiS_x/SUS (red) with JCPDS No. 01-089-7142 (NiS_2) and 03-065-3419 (NiS).

In order to investigate the chemical composition and binding states of the prepared electrodes, XPS analysis was carried out as shown in Figure 4. The XPS survey spectra of SUS, which mainly consists of Fe, Ni, Cr, and Mn, shows high intensity of O1s and C1s and very low intensity of Fe 2p indicating metal oxide film on SUS (Figure 4a) [23]. In case of S-SUS, because the intensity of Fe 2p and Cr 2p was too small to quantify the metal sulfides, S 2p was analyzed by the four peaks at 163.98 eV, 163.08 eV, 162.3 eV, and 161.2 eV (S_0, S_n^{2-}, S_2^{2-}, and S^{2-}) indicating the metal-S bonds (Figure S2) [24–26]. Therefore, it was elucidated that small amounts of metals were combined with sulfur on the surface of S-SUS. The survey spectra of NiS_x/SUS shows higher intensity of Ni 2p and S 2p compared to others. The low intensity of Fe 2p and Mn 2p is ascribed to minor metal diffusion during the synthesis. In order to confirm the binding states of NiS_x, the XPS result of NiS_x/SUS was presented by Ni 2p and S 2p deconvolution. The Ni 2p spectrum of the spin-orbit doublet was deconvoluted into six well-resolved peaks. As shown in Figure 4b, two major peaks are observed at 854.2 eV and 872.6 eV designated to Ni^{2+}, while the two peaks at 856.1 eV and 875.9 eV are attributed to Ni^{3+} in the Ni $2p_{1/2}$ and Ni $2p_{3/2}$ [27]. The elemental contents of SUS, S-SUS, and NiS_x/SUS are shown in Table S1. From this result, it was confirmed that the surface of the electrode was covered by NiS_x and no metallic nickel remained. The high resolution scan of S 2p is exhibited in Figure 4c. The binding states of S^{2-} and S_2^{2-} are observed at 161.2 eV and 162.3 eV respectively, which is indicative of NiS and NiS_2 [24]. These results are highly consistent with the XRD results of NiS_x/SUS, implying that the sulfurization was successful in synthesizing the hybrids of NiS and NiS_2 without metal diffusion from SUS during the synthesis.

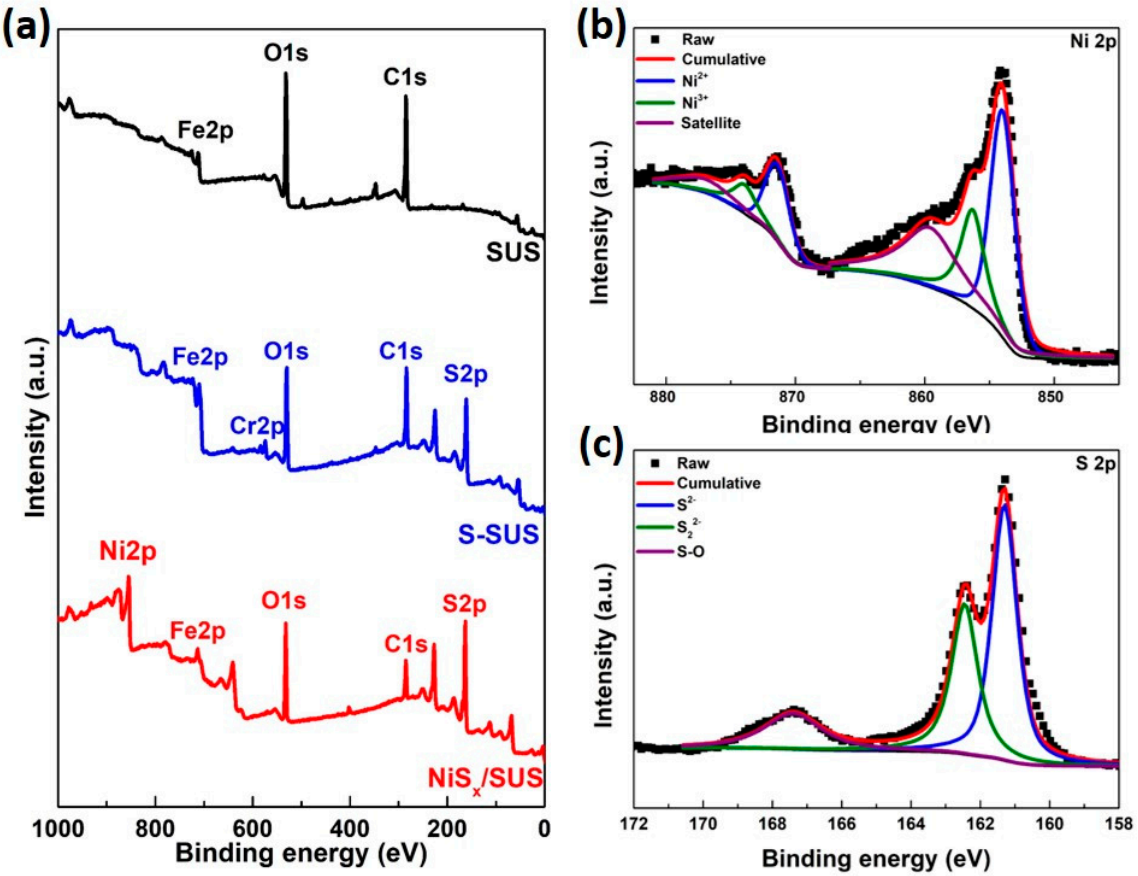

Figure 4. X-ray photoelectron spectroscopy of prepared electrodes. (**a**) Survey spectra of SUS (black), S-SUS (blue), and NiS_x/SUS (red); (**b**) high resolution XPS scans of Ni 2p; and (**c**) S 2p from NiS_x/SUS.

2.2. Electrochemical Results and Analysis

To investigate the HER performance of the prepared electrodes, a conventional three electrode experiment was performed in 1 M KOH. NiS_x/SUS was used as a working electrode, Pt and the saturated calomel electrode (SCE) were used as a counter electrode and reference electrode respectively. In order to see how much the HER performance was improved, SUS and S-SUS were used for the working electrodes as well. The polarization curve of NiS_x/SUS was considerably improved compared to SUS and S-SUS. For specific comparison we observed the η_{10} (overpotential at −10 mA cm^{-2}, mV vs reversible hydrogen electrode (RHE)) of each electrode (Figure 5a). The η_{10} of NiS_x/SUS was 258 mV, which is much smaller than those of S-SUS (494 mV) and SUS (457 mV). Tafel slope was used to understand the HER kinetics (Figure 5b,c). In general, the mechanism of HER in alkaline medium involves a two-step process [28]. The first step is the Volmer reaction ($H_2O + e^- \rightarrow H_{ads} + OH^-$) associated with the hydrogen adsorption on the electrocatalysts. The second step is the Heyrovsky ($H_2O + e^- + H_{ads} \rightarrow H_2 + OH^-$) or Tafel ($H_{ads} + H_{ads} \rightarrow H_2$) reaction which explain the H_2 dissociation from the electrocatalysts. Figure 5b shows that the Tafel slope of NiS_x/SUS was determined as 100 mV dec^{-1} which shows the improved electrocatalytic activity of NiS_x from the SUS. The Tafel slope reveals that the HER mechanism of NiS_x/SUS can be elucidated by the Volmer–Heyrovsky reaction as shown in Figure 5c. SUS and S-SUS show low Tafel slopes of 170 and 154 mV dec^{-1}, respectively, indicating poor electrocatalytic activity. As shown in the linear scan voltammetry (LSV) and Tafel plot, the HER performance of S-SUS was barely improved from the SUS even after sulfurization, which means the enhanced HER performance of NiS_x/SUS mainly stems from the NiS_x on the SUS. To better understand the electrocatalytic activities of the prepared electrode, double layer capacitances (C_{dl}) and electrochemical impedances were measured by cyclic voltammetry (CV) and electrochemical

impedance spectroscopy (EIS) experiments (Figure 5d,e). C_{dl} has a linear relationship with ECSA, which is correlated with the electrochemical performance of a given electrode (Figure 5d). Figure S3 shows the CV result obtained in the non-faradaic region at different scan rates (20 to 260 mV s^{-1}) for NiS_x/SUS, S-SUS, and SUS. S-SUS has 0.2 mF cm^{-2} for C_{dl} which is ten times higher than that of SUS (0.018 mF cm^{-2}) which is indicative of the similar trend with the LSV graph (Figure 5a). NiS_x/SUS show the highest C_{dl} value (2.63 mF cm^{-2}) which is 140 times higher than SUS and 13 times higher than S-SUS. For analysis of EIS, the Nyquist plot was used as shown in Figure 5e. All electrodes show the semicircles of the Nyquist plot and have similar R_s (solution resistance) around ~3 Ω in 1 M KOH. On the other hand, R_{ct} of NiS_x/SUS has the smallest value of 11.1 Ω, however, SUS and S-SUS show very high impedances (231.5 and 186.1 Ω). It was confirmed that the interfacial charge transfer reaction during the HER process occurs much more rapidly on the NiS_x/SUS than on the other electrodes.

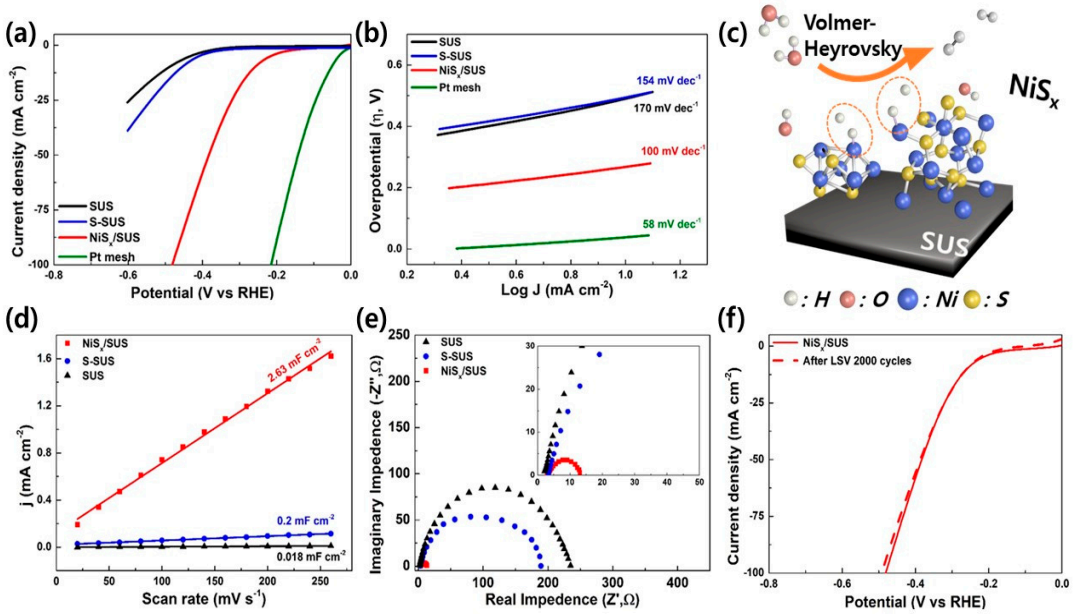

Figure 5. Hydrogen evolution reaction (HER) performances of prepared electrodes. (**a**) Linear scan voltammetry (LSV) in the range of 0 to −0.6 V vs reversible hydrogen electrode (RHE) in 1 M KOH; (**b**) Tafel plots; (**c**) illustration for hydrogen evolution reaction of NiS_x/SUS; (**d**) increased current density in non-faradaic region depending on the increasing scan rates for double layer capacitances of electrodes; (**e**) Nyquist plot at −0.4 V vs RHE; and (**f**) LSV 2000 cycles of NiS_x/SUS for 33 h.

In order to evaluate the electrochemical stability of NiS_x/SUS, the electrode was subjected to 2000 cycles of LSV (0 to −0.6 V vs RHE at 10 mV s^{-1}) for 33 h. As seen in Figure 5f, there is no significant difference in the LSV before and even after 2000 cycles, indicating the excellent long-term stability of the NiS_x/SUS. In addition to this, XPS results revealed that the NiS_x on NiS_x/SUS is stable after 2000 cycles of LSV in alkaline condition (Figure S4). These results imply high ECSA and low R_{ct} of NiS_x high corrosion resistance of SUS not only enhances the stability but also improves the HER performance in alkaline solution. Because SUS has slippery surface, electrodeposition was used for attachment of nickel on SUS for the stability of the electrode. To overcome the electrochemically poor activity of SUS, the ECSA of the electrode was considerably increased and R_{ct} was decreased by sulfurization of nickel on the SUS.

3. Materials and Methods

3.1. Preparation of Electrodes

Commercial stainless steel 304 (SUS, 10 mm × 20 mm × 250 μm) was used as a substrate for HER. DI water, ethanol, and acetone were used to clean the SUS subsequently. Nickel electrodeposition was carried out at −5 mA cm^{-2} for 30 min in 1 M nickel sulfate solution (Kanto, Tokyo, Japan). The deposited Ni on SUS was placed in the electric furnace for sulfurization. Ar gas (100 sccm) and sulfur powder (300 mg, Sigma Aldrich, St. Louis, MO, USA) were used as a carrier gas and an S precursor respectively. Sulfurization was carried out at 300 °C for 60 min in a low vacuum environment and the cooling temperature was controlled at a rate of 20 °C·min^{-1}. After synthesis, the electrode (denoted as NiS_x/SUS) was washed with acetone and dried at room temperature for 10 min. For comparison, SUS was sulfurized and dried, without electrochemically deposited nickel (denoted as S-SUS).

3.2. Characterizations

Field emission-scanning electron microscopy (FE-SEM; Hitachi, S-4300, Tokyo, Japan) was used to analyze the morphologies of NiS_x/SUS and S-SUS at the scale of 1 μm and 500 nm, respectively. The chemical composition and binding state of the electrode surface were confirmed through an XPS (Thermo Fisher Scientific Co, Waltham MA, USA) which had a micro-focused Al-Kα source. XRD (X'Pert PRO MRD, Phillips, Eindhoven, The Netherlands) analysis was carried out in the 2θ range of 20 to 90°.

3.3. Electrochemical Measurements

HER performance was evaluated by using potentiostat/galvanostat (Vertex, IVIUM Technology, Eindhoven, Netherlands) for a conventional three electrode system. To see the hydrogen evolution from alkaline solution, 1 M KOH was used as the electrolyte. The prepared electrodes, Pt and a saturated calomel electrode (SCE, Hg/Hg_2Cl_2) were used as working electrodes, a counter electrode, and a reference electrode respectively. LSV data were acquired in the range of 0 to −0.8 V vs RHE (versus reversible hydrogen electrode) at a scan rate of 10 mV s^{-1}, and CV experiments were carried at scan rates for every 20 mV s^{-1} increments up to a scan rate of 300 mV s^{-1} in the non-faradaic regions. The Nyquist plot was used for the analysis of EIS at the −0.4 V vs RHE in the frequency from 100k to 0.5 Hz. For a stability test, LSV 2000 cycles were carried out in the range of 0 to −0.6 V vs RHE at a scan rate of 10 mV s^{-1} for 33 h.

4. Conclusions

In this research, we overcame the limitations of SUS as a substrate and directly synthesized nickel sulfides through electrodeposition and sulfurization. The reported synthetic paradigm is very facile and straightforward, rendering the fabrication of the water splitting electrode at a large scale. Importantly, the NiS_x/SUS shows substantially improved HER kinetic performance in alkaline solution compared with SUS and S-SUS. The enhanced HER activity and long-term operational durability mainly stem from the increased ECSA of NiS_x/SUS and the high corrosion resistance of SUS. These results indicate that SUS substrate can be used for efficient HER with various electrocatalysts and nickel sulfides also can be synthesized on other substrates with the same methods.

Supplementary Materials: The following are available online at http://www.mdpi.com/2073-4344/10/11/1274/s1, contains supporting XPS and CV data. Figure S1: The thickness of the SEM image of NiS_x/SUS. Figure S2: Deconvolution of the XPS peaks of S-SUS in the S 2p region. Table S1: Surface chemical analysis of samples by X-ray photoelectron spectroscopy (XPS). Figure S3: CV of the prepared electrodes in the non-faradaic regions at different scan rates (20 mV s^{-1} to 260 mV s^{-1}). Figure S4: XPS of NiS_x/SUS after 2000 cycles in 1M KOH.

Author Contributions: K.-J.J. proposed the research direction and guided the project. J.-S.Y. carried out the conceptualization, methodology, data curation, Writing—original draft. S.J. carried out the conceptualization,

methodology, data curation, writing—review and editing. I.O. and S.P. carried out the methodology, writing—review and editing. H.D.M. carried out the data curation and writing—review and editing. All authors have read and agreed to the published version of the manuscript.

Funding: This work was supported by INHA UNIVERSITY Research Grant.

Conflicts of Interest: The authors declare no conflict of interest.

References

1. Shabanian, S.R.; Edrisi, S.; Khoram, F.V. Prediction and optimization of hydrogen yield and energy conversion efficiency in a non-catalytic filtration combustion reactor for jet A and butanol fuels. *Korean J. Chem. Eng.* **2017**, *34*, 2188–2197. [CrossRef]
2. Loipersböck, J.; Lenzi, M.; Rauch, R.; Hofbauer, H. Hydrogen production from biomass: The behavior of impurities over a CO shift unit and a biodiesel scrubber used as a gas treatment stage. *Korean J. Chem. Eng.* **2017**, *34*, 2198–2203. [CrossRef]
3. Kim, S.; Song, J.; Lim, H. Conceptual feasibility studies of a COX-free hydrogen production from ammonia decomposition in a membrane reactor for PEM fuel cells. *Korean J. Chem. Eng.* **2018**, *35*, 1509–1516. [CrossRef]
4. Roger, I.; Shipman, M.A.; Symes, M.D. Earth-abundant catalysts for electrochemical and photoelectrochemical water splitting. *Nat. Rev. Chem.* **2017**, *1*, 3. [CrossRef]
5. Wang, J.; Liu, J.; Zhang, B.; Ji, X.; Xu, K.; Chen, C.; Miao, L.; Jiang, J. The mechanism of hydrogen adsorption on transition metal dichalcogenides as hydrogen evolution reaction catalyst. *Phys. Chem. Chem. Phys.* **2017**, *19*, 10125–10132. [CrossRef]
6. Zhang, G.; Liu, H.; Qu, J.; Li, J. Two-dimensional layered MoS2: Rational design, properties and electrochemical applications. *Energy Environ. Sci.* **2016**, *9*, 1190–1209. [CrossRef]
7. Wei, W.; Mi, L.; Gao, Y.; Zheng, Z.; Chen, W.; Guan, X. Partial ion-exchange of nickel-sulfide-derived electrodes for high performance supercapacitors. *Chem. Mater.* **2014**, *26*, 3418–3426. [CrossRef]
8. Wang, Y.; Pang, H. Nickel-Based Sulfide Materials for Batteries. *ChemistrySelect* **2018**, *3*, 12967–12986. [CrossRef]
9. Wang, P.; Zhang, X.; Zhang, J.; Wan, S.; Guo, S.; Lu, G.; Yao, J.; Huang, X. Precise tuning in platinum-nickel/nickel sulfide interface nanowires for synergistic hydrogen evolution catalysis. *Nat. Commun.* **2017**, *8*, 1–9. [CrossRef]
10. Jayaramulu, K.; Masa, J.; Tomanec, O.; Peeters, D.; Ranc, V.; Schneemann, A.; Zboril, R.; Schuhmann, W.; Fischer, R.A. Nanoporous Nitrogen-Doped Graphene Oxide/Nickel Sulfide Composite Sheets Derived from a Metal-Organic Framework as an Efficient Electrocatalyst for Hydrogen and Oxygen Evolution. *Adv. Funct. Mater.* **2017**, *27*, 1–10. [CrossRef]
11. Wu, Y.; Gao, Y.; He, H.; Zhang, P. Novel electrocatalyst of nickel sulfide boron coating for hydrogen evolution reaction in alkaline solution. *Appl. Surf. Sci.* **2019**, *480*, 689–696. [CrossRef]
12. Palapati, N.K.R.; Demir, M.; Harris, C.T.; Subramanian, A.; Gupta, R.B. Enhancing the electronic conductivity of Lignin-sourced, sub-micron carbon particles. In Proceedings of the 2015 IEEE Nanotechnology Materials and Devices Conference (NMDC), Anchorage, AK, USA, 13–16 September 2015; pp. 1–2. [CrossRef]
13. Hung, T.F.; Yin, Z.W.; Betzler, S.B.; Zheng, W.; Yang, J.; Zheng, H. Nickel sulfide nanostructures prepared by laser irradiation for efficient electrocatalytic hydrogen evolution reaction and supercapacitors. *Chem. Eng. J.* **2019**, *367*, 115–122. [CrossRef]
14. Liu, P.; Li, J.; Lu, Y.; Xiang, B. Facile synthesis of NiS2 nanowires and its efficient electrocatalytic performance for hydrogen evolution reaction. *Int. J. Hydrogen Energy* **2018**, *43*, 72–77. [CrossRef]
15. TONG, S.S.; WANG, X.J.; LI, Q.C.; HAN, X.J. Progress on Electrocatalysts of Hydrogen Evolution Reaction Based on Carbon Fiber Materials. *Chinese J. Anal. Chem.* **2016**, *44*, 1447–1457. [CrossRef]
16. Benck, J.D.; Pinaud, B.A.; Gorlin, Y.; Jaramillo, T.F. Substrate selection for fundamental studies of electrocatalysts and photoelectrodes: Inert potential windows in acidic, neutral, and basic electrolyte. *PLoS ONE* **2014**, *9*. [CrossRef] [PubMed]
17. Pu, N.W.; Shi, G.N.; Liu, Y.M.; Sun, X.; Chang, J.K.; Sun, C.L.; Der Ger, M.; Chen, C.Y.; Wang, P.C.; Peng, Y.Y.; et al. Graphene grown on stainless steel as a high-performance and ecofriendly anti-corrosion coating for polymer electrolyte membrane fuel cell bipolar plates. *J. Power Source* **2015**, *282*, 248–256. [CrossRef]

18. Kim, M.; Ha, J.; Shin, N.; Kim, Y.T.; Choi, J. Self-activated anodic nanoporous stainless steel electrocatalysts with high durability for the hydrogen evolution reaction. *Electrochim. Acta* **2020**, *364*, 137315. [CrossRef]
19. Kovendhan, M.; Kang, H.; Youn, J.S.; Cho, H.; Jeon, K.-J. Alternative cost-effective electrodes for hydrogen production in saline water condition. *Int. J. Hydrogen Energy* **2018**, *44*, 5090–5098. [CrossRef]
20. Kovendhan, M.; Kang, H.; Jeong, S.; Youn, J.S.; Oh, I.; Park, Y.K.; Jeon, K.J. Study of stainless steel electrodes after electrochemical analysis in sea water condition. *Environ. Res.* **2019**, *173*, 549–555. [CrossRef]
21. Zhu, W.; Yue, X.; Zhang, W.; Yu, S.; Zhang, Y.; Wang, J.; Wang, J. Nickel sulfide microsphere film on Ni foam as an efficient bifunctional electrocatalyst for overall water splitting. *Chem. Commun.* **2016**, *52*, 1486–1489. [CrossRef] [PubMed]
22. Quan, C.; He, Y. Properties of nanocrystalline Cr coatings prepared by cathode plasma electrolytic deposition from trivalent chromium electrolyte. *Surf. Coatings Technol.* **2015**, *269*, 319–323. [CrossRef]
23. Jung, R.H.; Tsuchiya, H.; Fujimoto, S. XPS characterization of passive films formed on Type 304 stainless steel in humid atmosphere. *Corros. Sci.* **2012**, *58*, 62–68. [CrossRef]
24. Limaye, M.V.; Chen, S.C.; Lee, C.Y.; Chen, L.Y.; Singh, S.B.; Shao, Y.C.; Wang, Y.F.; Hsieh, S.H.; Hsueh, H.C.; Chiou, J.W.; et al. Understanding of sub-band gap absorption of femtosecond-laser sulfur hyperdoped silicon using synchrotron-based techniques. *Sci. Rep.* **2015**, *5*, 1–12. [CrossRef]
25. Demir, M.; Farghaly, A.A.; Decuir, M.J.; Collinson, M.M.; Gupta, R.B. Supercapacitance and oxygen reduction characteristics of sulfur self-doped micro/mesoporous bio-carbon derived from lignin. *Mater. Chem. Phys.* **2018**, *216*, 508–516. [CrossRef]
26. Altinci, O.C.; Demir, M. Beyond Conventional Activating Methods, a Green Approach for the Synthesis of Biocarbon and Its Supercapacitor Electrode Performance. *Energy Fuels* **2020**, *34*, 7658–7665. [CrossRef]
27. Nis, S.D.; Catalysis, E. Solvothermally Doping NiS2 Nanoparticles on Carbon with Ferric Ions for E ffi cient Oxygen Evolution Catalysis. *Catalysts* **2019**, *9*, 458. [CrossRef]
28. Tian, X.; Zhao, P.; Sheng, W. Hydrogen Evolution and Oxidation: Mechanistic Studies and Material Advances. *Adv. Mater.* **2019**, *31*, 1–7. [CrossRef] [PubMed]